

Journal of Basics and Applied Sciences Research (JOBASR) ISSN (print): 3026-9091, ISSN (online): 1597-9962 Volume 1(1) IPSCFUDMA 2025 Special Issue

DOI: https://dx.doi.org/10.4314/jobasr.v1i1.10s



# Anti-corrosion Properties of *Piliostigma Thonningi* Leave Extract-Transition Metal Nano Particle Composites on Mild Steel in 1.0m Hydrochloric Acid Solution

Ameh Ojochide Monday<sup>1</sup>, Chahul Faith Habibat<sup>2</sup>, Wuana Raymond Ahulle<sup>2</sup>

<sup>1</sup>Department of Chemistry, Federal University Dutsin-Ma, Katsina State.

<sup>2</sup>Joseph Sarwun Tarka University, Makurdi.

\*Corresponding Author Email: aojochide@fudutsinma.edu.ng

#### **ABSTRACT**

Ethanolic extract of *Piliostigma thonningii* was employed to synthesise silver and titanium nanoparticle composites. The particle sizes of the AgNPs and TiNPs were analysed and characterized via ultraviolet-visible spectroscopy, Fourier Transform Infrared spectroscopy, Scanning Electron Microscopy/Energy Dispersive X-ray and X-ray Diffraction. The result from the ultraviolet-spectroscopy showed a maximum absorption around (400-470 nm) for the AgNPs compared to TiNPs (270-350nm). The Fourier transformed infrared spectra showed maximum. Prominent peaks corresponded to C=C, N-H, O-H and C=O functionalities, these groups facilitated strong adsorption onto the mild steel surface through hydrogen bonding, metal-ligand coordination, and  $\pi$ -electron interactions, leading to the formation of a protective film with effective inhibition. The Scanning Electron Microscopy/Energy Dispersive Xray analysis showed a progressive improvement in the surface morphology from the blank, PTE, PTE-AgNPs, and PTE-TiNPs samples. The PTE-nanoparticles composites, especially PTE-AgNPs, provided superior surface protection, confirming their effectiveness as corrosion inhibitors in 1.0 M solution. The Xray Diffraction showed that the nanoparticles were around 38.62nm to 70.59nm in size, as derived from the Debye Scherrer equation  $d\text{-}\frac{0.89\lambda}{\beta cos\theta}$  . The anticorrosion properties of the NPs for mild steel in 1.0 M HCl at 303-333K were studied using weight loss and electrochemical measurements. Both AgNPs and TiNPs were found to exhibit anti-corrosive properties against the dissolution of the steel coupons in the acidic electrolyte, with corrosion inhibitive effects found to be concentration and temperature dependent. The synthesized AgNPs displayed a higher inhibition efficiency (95.1%) at an optimum concentration of 0.10g/L compared with TiNPs (91.2%) and the plant extract (87.7 %). Potentiodynamic polarization results showed that the understudied nanoparticles behaved as mixed-type inhibitors, inhibiting the anodic dissolution of the mild steel and cathodic evolution of hydrogen gas. The plant-derived NPs adsorbed on the surface of mild steel via a physical adsorption mechanism as predicted by the

#### **Keywords:**

Piliostigma thonningii, nanoparticles, mild steel, electrochemical impedance spectroscopy.

#### INTRODUCTION

Corrosion remains a major challenge in industrial sectors such as construction, oil and gas, marine, and chemical processing, particularly in acidic environments where mild steel is commonly used (7);(18). Despite its favorable mechanical and economic attributes, mild steel is prone to rapid corrosion in acids like 1.0 M HCl, often used for descaling, cleaning, and pickling operations. To address this issue, corrosion inhibitors are typically employed to reduce metal dissolution and surface degradation (14).

Green corrosion inhibitors derived from plant extracts have garnered significant attention due to their environmental safety and biodegradability compared to conventional toxic inhibitors such as chromates and nitrates (7);(15); (18). Plant extracts are rich in phytochemicals like flavonoids, alkaloids, tannins, terpenoids, and phenolics, which can adsorb onto metal surfaces and form protective films (21). For example, Dysphania ambrosioides essential oil achieved over 84% inhibition for mild steel in 1.0 M HCl (16). Similarly, (33) reported inhibition efficiencies above

Langmuir adsorption isotherm model..

90% using Ganoderma lucidum and black mustard seed extracts due to strong adsorption via nitrogen and oxygen heteroatoms. However, the use of plant extracts alone faces challenges such as limited thermal stability and short-term protection under harsh conditions (19), prompting research into nanoparticle integration. Nanoparticles enhance the performance of plant-based inhibitors due to their high surface area and active chemistry, enabling them to form dense and adherent films on metal surfaces. Silver nanoparticles (AgNPs) are among the most studied in this context. (13) demonstrated that AgNPs synthesized with Anacardium occidentale leaf extract provided 90% inhibition efficiency at 80 °C in seawater. Furthermore, bioengineered AgNPs with plant proteins reduced corrosion rates from 2.2 mm/year to 0.5 mm/year in cooling systems (28). Other effective nanoparticles include ZrO<sub>2</sub>, NiO, and TiO<sub>2</sub>. ZrO<sub>2</sub>-glycine nanocomposites achieved 81% inhibition in 1.0 M HCl at 70 °C and followed the Langmuir isotherm (19). TiO<sub>2</sub> nanoparticles derived from Chromolaena odorata also significantly enhanced corrosion resistance for mild steel (24); (29).

The enhanced performance of plant extract-nanoparticle composites is attributed to synergistic interactions at the metal–solution interface. Phytochemicals adsorb through  $\pi$ -electrons and lone pair-bearing heteroatoms (N, O, S), while nanoparticles fill surface voids and reinforce chemisorbed layers (22); (27); (33). These systems typically exhibit mixed-type inhibition, affecting both anodic and cathodic reactions (19). Electrochemical methods such as EIS and potentiodynamic polarization confirm improved charge transfer resistance and reduced corrosion current densities when nanoparticles are used in combination with plant extracts.

The 1.0 M HCl medium remains a widely accepted standard for evaluating corrosion inhibitors due to its industrial relevance. Studies such as those by (31) and (19) have shown that composites like chitosan–AgNPs and ZrO<sub>2</sub>–glycine nanocomposites maintain effective corrosion inhibition across varying temperatures and acid concentrations, confirming their practical applicability.

Despite growing interest, *Piliostigma thonningii*, a West African plant rich in flavonoids, tannins, and phenolics (7), has been underexplored as a corrosion inhibitor. These phytochemicals not only serve as reducing/stabilizing agents for nanoparticles but also possess inherent inhibition properties. Combining *P. thonningii* leaf extract with transition metal nanoparticles is anticipated to yield a thermally stable, cost-effective, and eco-friendly inhibitor suitable for acidic media like 1.0 M HCl.

The aim and objectives of this study was to investigate the anti-corrosion properties of piliostigma thonningii leaves transition metal nanoparticles composite on mild steel in 1.0 M HCl solution

#### MATERIALS AND METHODS

#### Materials and measurements

The solvents and reagents used were purchased from Merck and Sigma-Aldrich, and used without further purification.

# Preparation of Plant Leaves Extracts Transition Metal Nanoparticles (PTM-NPs)

Piliostigma thonningii leaves were washed, dried in an oven at 313 K for 24 hours, before being crushed with an electric blender. Ten grams of the crushed leaves were extracted using n-hexane, ethyl acetate, and ethanol, concentrated with a rotary evaporator, filtered, and refrigerated for later use. The procedure for synthesizing PTM-NPs is similar to that described by (19) and (24). In an Erlenmeyer flask, 80 mL of 1.0 M titanium (IV) chloride and silver nitrate were mixed with 20 mL of freshly prepared Piliostigma thonningii extract (PTE) each, and stirred for 1 hour at room temperature using a homogenization stirrer at 4000 rpm. Colour transitions were observed both visually and using UV/Vis spectroscopy (JASCO 630), confirming the formation of nanoparticles as described by (26). The nanoparticles were centrifuged for 30 minutes at 6000 rpm. To obtain powdered nanoparticles, the settling solid residues were washed twice with double-distilled water, re-dissolved in absolute ethanol, and evaporated to dryness at 353 K. following a methodology similar to that reported by

# **Characterisation of Plant Extract-Transition Metal Nanoparticles (PTM-NPs)**

The prepared plant-nanoparticle hybrids were characterised using both classical and instrumental methods. A JASCO 680 UV-visible spectrophotometer was used to determine the surface plasmon resonance confirming nanoparticle formation, (SPR), commonly observed in green-synthesised nanomaterials (6). An Agilent Cary 630 FT-IR spectrometer was employed to identify the functional groups present in the PTM-NPs before and after corrosion exposure, aiding in the determination of whether the interaction involved chemisorption, physisorption, or both (29).

Surface morphology were investigated using a Scanning Electron Microscope (Model: X:PRO:X:800-07334, Phenom World, S/N: MVEO1570775) equipped with Energy Dispersive X-ray Spectroscopy (EDS), which provided insights into electron interactions and the resulting topographical and compositional data (11). X-ray diffraction (XRD) analysis was conducted using a Thermo Scientific X-ray Diffractometer (Model: ARL'XTRA X-ray, S/N: 197492086) to determine the crystalline nature and grain size of the synthesised PTM-NPs (9).

These techniques provided a comprehensive understanding of the morphology, surface functional groups, and stability of the nanoparticles, which are essential for evaluating their anticorrosive performance and interaction mechanisms.

#### **Anticorrosion Studies**

The mild steel sheets used for this study was obtained commercially from pipeline construction market in Kaduna, Nigeria. They were mechanically cut into dimensions of 2 cm x 3 cm x 1cm for both weight loss and electrochemical experiments. The coupons were wet polished with silicon carbide abrasive paper, degreased in ethanol, dried with acetone and warm air, weighed, and stored in a moisture-free desiccator before usage.

PTE, PTE-TMNPs were used as corrosion inhibitors in the concentrations range of 0.02 g/L, 0.04 g/L, 0.06 g/L, 0.08 g/L and 0.10 g/L and tested for their adsorptive and inhibitive properties. The pre-weighed mild steel coupons were immersed in 1.0 M HCl solution without and with different concentrations of the Plant leaf extracts, and Plant leave extract-Nano particle for one hour at 303 K, 313K, 323K and 333K in a water bath. They were retrieved, cleaned and re-weighed to determine the weight loss. This experiment was carried out in duplicates and the mean values of the weight losses (g) were used for computation of corrosion rate (CR) and inhibition efficiency IE (%) using Equation (1) and (2) below:

Corrosion Rate = CR (mmy<sup>-1</sup>) = 
$$\frac{87.6 \times \Delta W}{\rho AT}$$

were  $\Delta W$  is the weight loss,  $C_{R(blank)}$  and  $C_{R(Inhibitor)}$  are the corrosion rates (mm/yr.) in the absence and presence of the Plant Extract-Nano particles,  $\rho$  and A depict the density and average surface area (cm<sup>2</sup>) of the coupon while T is the immersion time (h). This procedure was repeated at 313, 323 and 333 K for the different test solutions.

#### **Electrochemical Measurements**

The electrochemical measurement was carried out by using a three-electrode system consisting of working electrode (mild steel coupon), reference electrode (saturated calomel) and a counter electrode (platinum). The selected concentration for the PTM-NPs was 0.02g/L. The instrument used for the electrochemical analysis was the VMP Biologic, SP 300 model. The Tafel polarization plots of potential Vs, the current density was recorded, in the given potential range of -0.28V to -0.50V at a scan rate of 1mV/s. The electrochemical impedance spectra were recorded by using AC signals with amplitude

0.01V/s at OCP in the frequency range from 100 kHz to 0.1 Hz. Data fitting and analyses were done using Origin package. The inhibition efficiency was calculated from the values of charge transfer resistances and corrosion current densities from EIS and the PDP values according to Equation (3) and (4) below respectively

$$IE_{EIS} = (1 - \frac{R_{ct}^0}{R_{ct}}) x 100$$

Where  $R_{Ct}^0$  and  $R_{Ct}$  are charge transfer resistances in the absence and presence of the inhibitor respectively.

$$IE_{PDP} = (1 - \frac{i_{corr}}{i_{corr}^0}) \times 100$$

Where  $I_{corr}^0$  and  $I_{corr}$  are the corrosion current densities in the absence and presence of the inhibitor respectively.

#### RESULTS AND DISCUSSION

#### **Ultraviolet-visible Analyses**

The adsorption spectrum is depicted in Figures 1 and 2, showing the UV-visible spectrum recorded for the synthesized PTM-NPs. It can be observed that the surface plasmon resonance (SPR) bands appear within 400–470 nm for PTE-AgNPs and 270–350 nm for PTE-TiNPs. The peaks of the plant extract-thinsition metal nanoparticles may be attributed to the spectral absorptions of phenolic compounds present in the plant extract-mediated nanoparticles (6); (20).

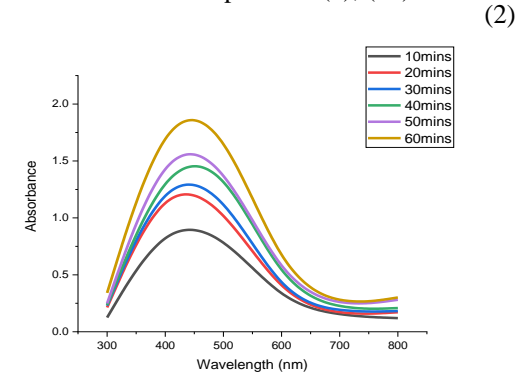


**Figure1.** UV-vis spectrum of developed PTE-AgNPs at different time intervals

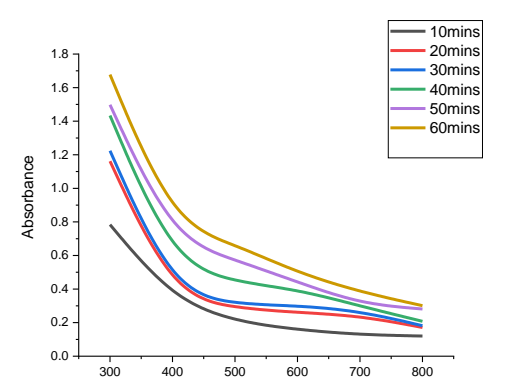


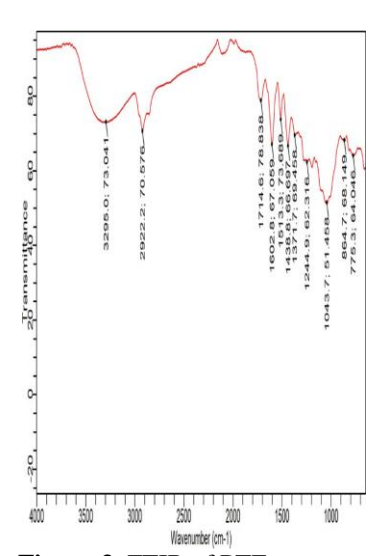
Figure 2. UV-vis spectrum of developed PTE-TiNPs at different time intervals

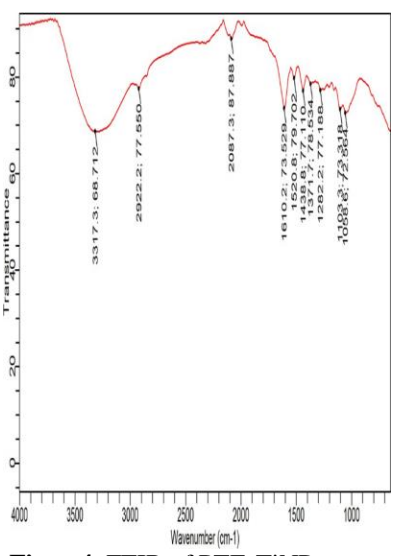
Wavelength (nm)

#### **FTIR Analyses**

Ojochide et al.

Figure 3 to 5 shows the FTIR spectra of the inhibitors, the FTIR analysis showed key functional groups in the plant extract (PTE), including hydroxyl (O-H) and carbonyl (C=O) groups, which played a vital role in the reduction and stabilization of titanium and silver nanoparticles. Shifts in peak positions and the appearance of new bands corresponding to Ti-O and Ag-O confirmed successful nanoparticle synthesis. These spectral changes indicate strong interactions between the phytochemicals and the nanoparticles, validating green synthesis. The FTIR results confirmed the presence of phytochemicals that cap TiNPs and AgNPs, enhancing stability and surface activity. These functional groups aid in forming protective films on the Mild Steel surfaces, contributing to the nanoparticles effectiveness at green anti-corrosion agents.





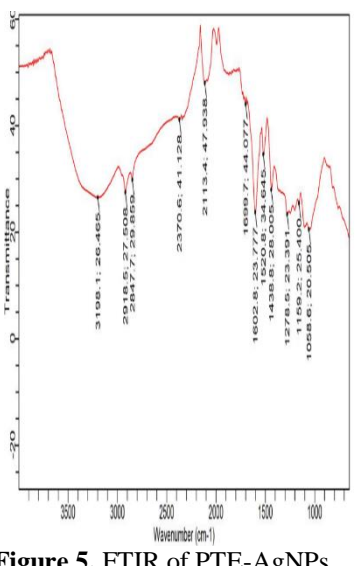


Figure 3. FTIR of PTE

Figue 4. FTIR of PTE-TiNPs

Figure 5. FTIR of PTE-AgNPs

#### X-ray Diffraction (XRD) Analyses

The XRD pattern shows different diffraction peaks at 2theta (deg.). The sharp peaks confirm the crystallinity of the PTM-NPs and the average crystalline (grain) size for each of the plant extracts transition metal nanoparticles were determined using Debye Scherrer Equation (5) below

$$d = \frac{0.89\lambda}{\beta \cos \theta}$$

The values obtained were 57.12nm, 65.61nm for PTE-AgNPs and PTE-TiNPs. The higher intense peaks and absence of unidentified peaks confirmed the higher purity of the prepared nanoparticles. (12)

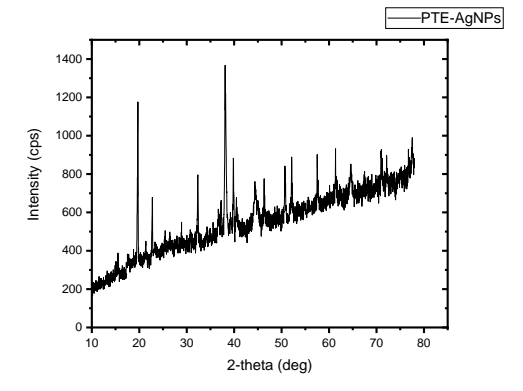


Figure 6. XRD pattern of PTE-AgNPs

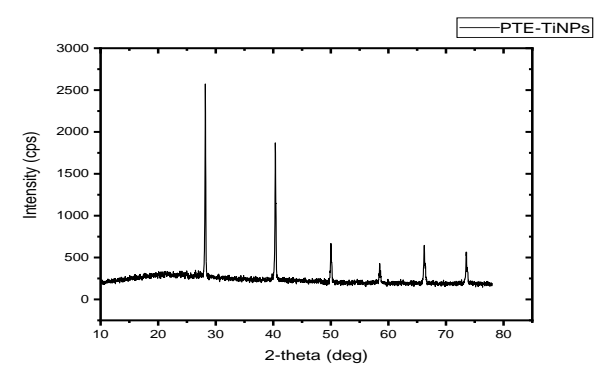


Figure 7. XRD Pattern of PTE-TiNPs

# Plate 2. Blank (no inhibitor), Plate 3. PTE-treated, Plate 4. PTE-AgNPs-treated, and Plate 5 PTE-TiNPs-treated samples. The blank sample exhibits severe surface degradation with visible corrosion pits and cracks, while the PTE-treated surface shows partial film formation and moderate corrosion. The PTE-AgNPs sample reveals a smooth and compact protective layer with minimal surface damage, indicating strong inhibitor performance. The PTE-TiNPs surface also shows reduced corrosion with a relatively uniform film, though less compact than the AgNP-based system.

#### **SEM Analysis**

The SEM micrographs of mild steel surfaces after 6 hours immersion in 1.0 M HCl solution is shown in plate 2 to 5.

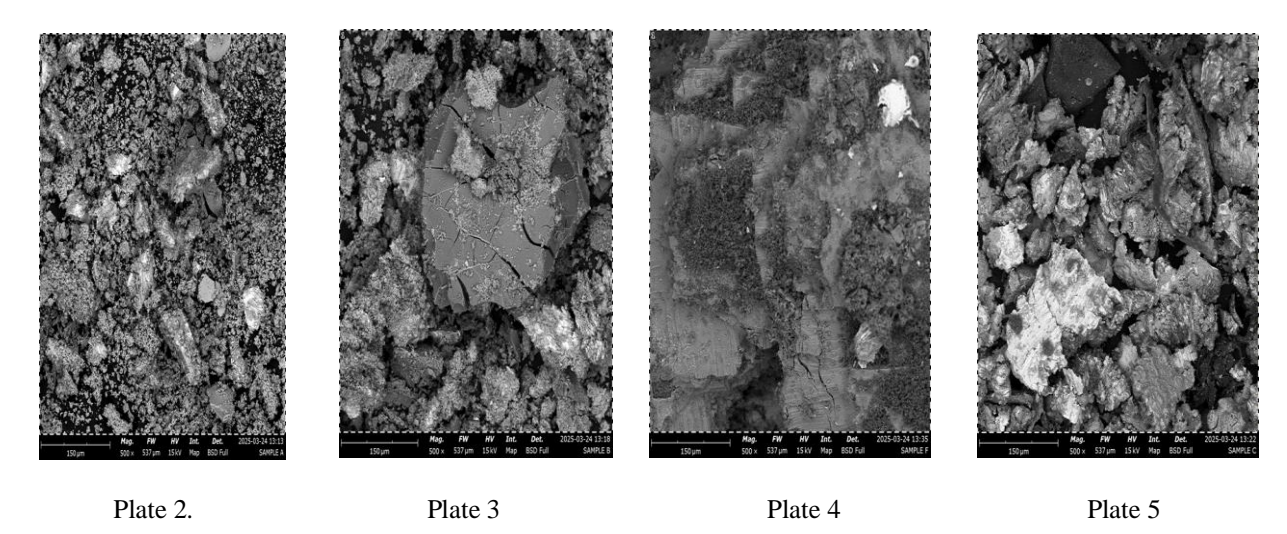


Plate 2. SEM of Mild Steel in 1.0M solution without inhibitor

Plate 3. SEM of Mild Steel in 1.0M solution in the presence of PTE

Plate 4. SEM of Mild Steel in 1.0M solution in the presence of PTE-TiNPs

Plate 5. SEM of Mild Steel in 1.0 M solution in the presence of PTE-AgNPs

# **Anti-corrosion activities:**

The efficiency of corrosion inhibitors, including plant-based extracts and nanoparticle composites, is influenced significantly by both their concentration and the operating temperature. At lower concentrations, the corrosion rate of mild steel tends to be higher due to incomplete surface coverage. As the inhibitor concentration increases, corrosion rates generally decrease due to improved adsorption and formation of a more compact and protective barrier film on the metal surface (1); (26). However, temperature plays a critical role in modifying this interaction. An increase in temperature typically leads to a decline in inhibition efficiency. This is primarily due to the thermal desorption or decomposition of the

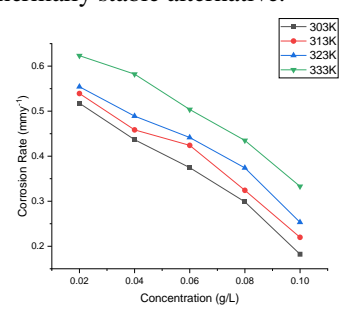
inhibitor film, which compromises its protective capacity even at elevated concentrations (19); (24). The thermal instability of organic molecules and the breakdown of weakly adsorbed layers at higher temperatures result in increased corrosion rates, as fewer active species remain bonded to the metal surface (17).

Figures 8 to 10 illustrate the combined effect of temperature and additive concentration on the corrosion rate of mild steel coupons in an acidic aqueous environment. These trends confirm that while increased inhibitor concentration improves protection, elevated temperatures offset this gain by destabilizing the inhibitor film. Figures 11 to 14 further demonstrate the inhibition efficiency of *Piliostigma thonningii* leaf

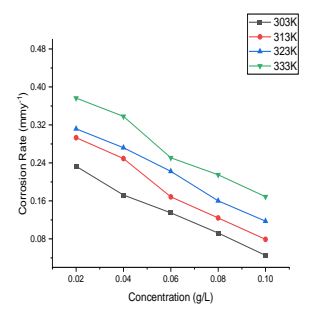
#### Anti-corrosion Properties of Piliostigma ...

extract (PTE) and its synthesized nanoparticle composites (PTE-AgNPs and PTE-TiNPs) at varying temperatures in 1.0 M HCl solution. Figure 15 presents the influence of increasing concentrations of PTE, PTE-AgNPs, and PTE-TiNPs on the corrosion rate of mild steel in 1.0 M HCl, while Figure 16 shows the corresponding inhibition efficiencies at 303 K. A notable trend observed is that nanoparticle composites, especially those containing titanium and silver, maintain relatively higher inhibition efficiencies at elevated temperatures compared to plant extract alone. This is attributed to the improved thermal stability, surface interaction, and film-forming capacity of metal nanoparticles (13); (31).

Table 1 compares the inhibition efficiencies (IE%) of 0.10 g/L PTE, PTE-AgNPs, and PTE-TiNPs in 1.0 M HCl solution. It confirms that nanoparticle-functionalized plant extracts exhibit superior performance across different temperatures, validating the synergy between phytochemicals and metal nanoparticles in enhancing corrosion resistance. Therefore, it can be concluded that the corrosion inhibition performance of these additives is highly dependent on both concentration and operational temperature, with nanoparticle inclusion offering a more robust and thermally stable alternative.

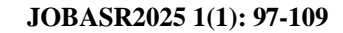


**Figure 8.** The effect of temperature on the corrosion rate in the presence of different concentration of PTE in 1.0M HCl



**Figure 9.** Corrosion Rate against Concentration of PTE-AgNPs at different Temperature (K) in 1.0M HCl

# Ojochide et al.



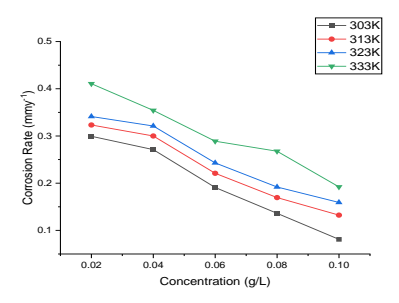


**Figure 10.** Corrosion Rate against Concentration of PTE-AgTi at different Temperature in 1.0M HCl

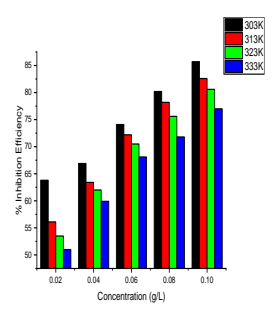


**Figure 11.** Effect of Concentration on Inhibition efficiency of PTE at different Temperature (K) in 1.0M HCl

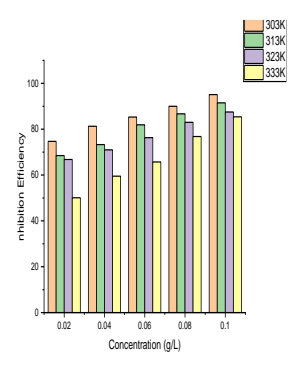


**Figure 12.** Effect of Concentration on Inhibition efficiency of PTE-AgNPs at different Temperature (K) in 1.0M HCl

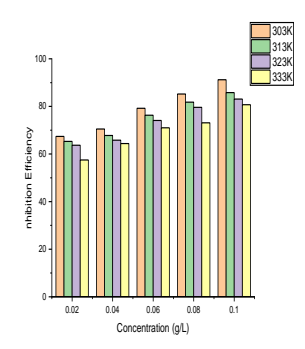


**Figure 13.** Effect of Concentration on Inhibition efficiency of PTE-TiNPs at different Temperature (K) in 1.0M HCl

mild steel in the presence of PTE, PTE-AgNPs and PTE-TiNPs in 1.0 M HCl at 303K

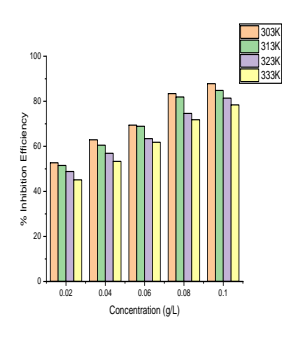
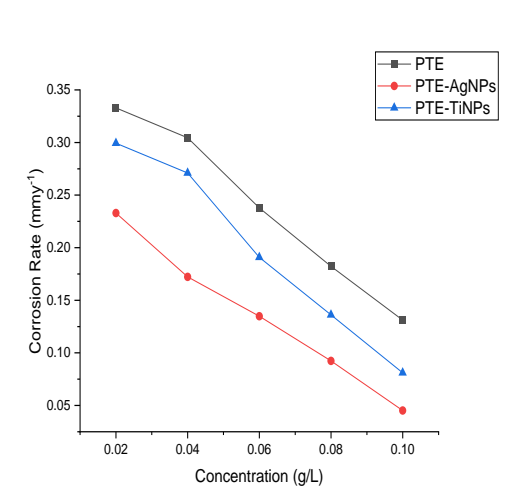


**Figure 14.** Effect of Concentration on Inhibition efficiency of PTE-TiNPs at different Temperature (K) in 1.0M HCl solution



PTE-AgNPs
PTE-TINPs

PTE-TINPs

Output

**Figure 16.** Effect of concentration on Inhibition efficiency of mild steel in the presence of PTE, PTE-AgNPs and PTE-TiNPs in 1.0 M HCl at 303K

Figure 15. Effect of concentration on Corrosion rate of

Table 1: Comparison of (%) inhibition efficiency of 0.10g/L PTE, PTE-AgNPs, and PTE-TiNPs in 1.0M HCl

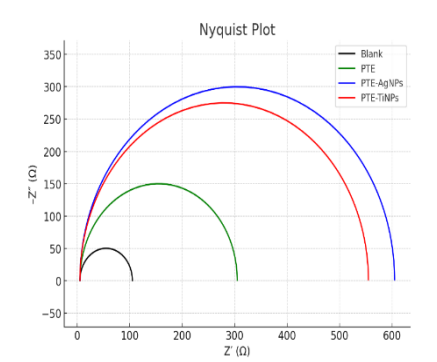
S/N	INHIBITION EFFICIENCY (%)					
	TEMPERATURE	PTE	PTE-AgNPs	PTE-TiNPs		
	(K)		_			
1	303	87.7	95.1	91.2		
2	313	82.6	91.5	85.8		
3	323	80.6	87.5	83.1		
4	333	77.0	83.1	80.7		

# Electrochemical Impedance Spectroscopy (EIS) Measurement

The electrochemical impedance spectroscopy (EIS) results provided significant insights into the corrosion behavior of the mild steel in 1.0 M HCl solution in the presence and absence of plant-based inhibitors. Nyquist plots revealed depressed semicircular arcs indicative of charge transfer controlled processes, with the diameter of the semicircles increasing markedly upon addition of inhibitors. The blank sample exhibited the smallest arc, reflecting low charge transfer resistance (Rct) and a high corrosion rate. Upon the addition of plant extract (PTE), Rct increased moderately, and suggesting partial surface coverage by bioactive molecules. However, the incorporation of silver and titanium nanoparticles (PTE-

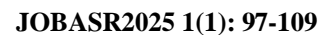
AgNPs and PTE-TiNPs) substantially enhanced corrosion resistance, as evidenced by much larger semicircle diameters. Bode plots further confirmed these observations, where both the impedance magnitude (|Z|) and phase angle were significantly for the nanoparticle based higher particularly PTE-AgNPs. The broader phase angle maxima and higher impedance at low frequencies indicated the formation of a more capacitive and protective layer on the steel surface. Overall, the EIS data demonstrate that PTE-AgNPs provided the most effective barrier against corrosion, attributed to improved adsorption, film compactness, and synergistic inhibition mechanisms.

# Anti-corrosion Properties of Piliostigma ...



**Figure 17.** Nyquist plot for anticorrosion study of Mild steel coupon in 1.0 M HCl solution in the absence and presence of inhibitors (PTE, PTE-AgNPs, PTE-TiNPs)

# Ojochide et al.



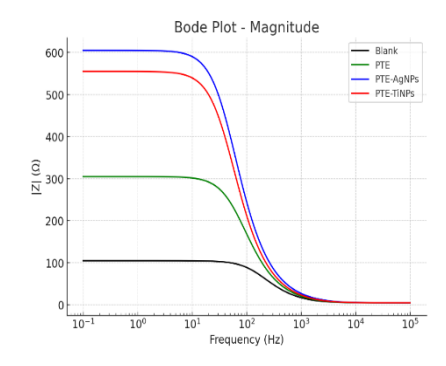


**Figure 18.** Bode plot for anticorrosion study of Mild steel coupon in 1.0 M HCl solution in the absence and presence of inhibitors (PTE, PTE-AgNPs, PTE-TiNPs)

#### **Adsorption Isotherm**

The PTM-NPs adsorption all fitted into Langmuir adsorption model in figure 19 and 21. Table 2 and 4 shows the Langmuir adsorption isotherm for adsorption of PTM-NPs. While Table 3 and 5 shows the parameters deduced from the Langmuir adsorption isotherm for adsorption of PTM-NPs (32).

Table 2. Langmuir adsorption isotherm for adsorption of PTE-AgNPs Parameters

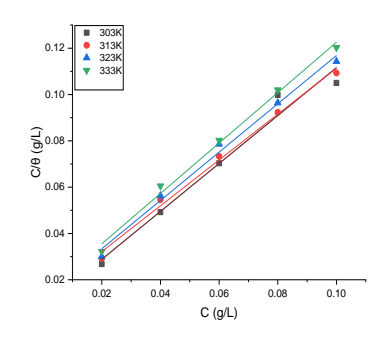
S/N	Concentration	303K	313K	323K	333K
		C/θ	С/θ	С/θ	С/θ
1	0.02	0.0268	0.0292	0.0300	0.0322
2	0.04	0.0492	0.0546	0.0563	0.0605
3	0.06	0.0703	0.0733	0.0786	0.0802
4	0.08	0.0998	0.0923	0.0964	0.1020
5	0.10	0.1050	0.1093	0.1143	0.1203

Table 3. Parameters deduced from the PTE-AgNPs Langmuir adsorption isotherm plot

Temp. (K)	$\Delta G_{ads}(kJmol^{-1})$	$K_{ads} (Lg^{-1})$	Intercepts	Slope	$R^2$	
303	-17.315	0.966	0.008	1.035	0.971	
313	-17.979	1.001	0.012	0.999	0.994	

Anti-corrosion Properties of Piliostigma		Ojochide et al.	JOBASR2025 1(1): 97-109		
323	-18.432	0.957	0.013	1.044	0.992
333	-18.888	0.918	0.014	1.089	0.994

# concentrations of PTE-AgNPs



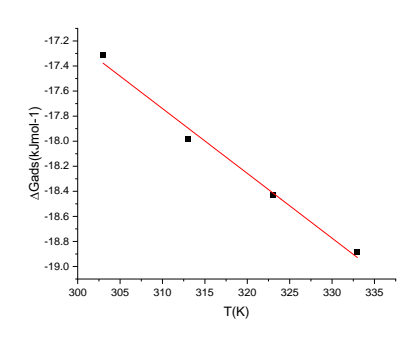


Figure 19. Variation of  $C/\theta$  with concentration for the corrosion of mild steel in 1.0 M HCl containing various

Figure 20. Plot of  $\Delta G^0_{ads}$  against T for the adsorption of PTE-AgNPs

Table 4. Langmuir adsorption isotherm for adsorption of PTE-TiNPs Parameters

S/N	Concentration	303K	313K	323K	333K	_
		C/θ	C/θ	C/θ	C/θ	
1	0.02	0.0297	0.0306	0.0314	0.0348	
2	0.04	0.0567	0.0590	0.0608	0.0621	
3	0.06	0.0758	0.0786	0.0810	0.0845	
	3.00	0.0720	0.0700	0.0010	0.00 12	
4	0.08	0.0939	0.0978	0.1005	0.1094	
5	0.10	0.1097	0.1166	0.1203	0.1239	
5	0.10	0.1097	0.1100	0.1203	0.1239	

**Table 5.** Parameters deduced from the PTE-TiNPs Langmuir adsorption isotherm plot

Temp. (K)	$\Delta G_{ads}(kJmol^{-1})$	$K_{ads} (Lg^{-1})$	Intercepts	Slope	$\mathbb{R}^2$
303	-17.437	1.014	0.014	0.986	0.989
313	-17.840	0.949	0.013	1.054	0.992
323	-18.323	0.919	0.014	1.088	0.992

333 -18.793 0.887 0.015 1.128 0.990

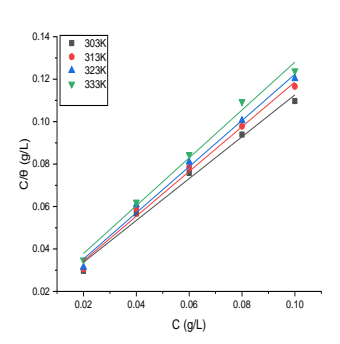


**Figure 21.** Variation of  $C/\theta$  with concentration for the corrosion of mild steel in 1.0 M HCl containing various concentrations of PTE-TiNPs

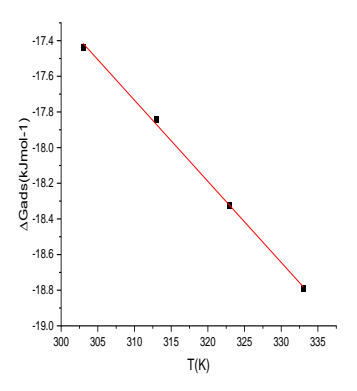


**Figure 22.** Plot of  $\Delta G^0_{ads}$  against T for the adsorption of PTE-TiNPs

# Kinetic and Thermodynamic Studies

Figure 20 and 22 shows the Plot of  $\Delta G^0_{ads}$  against T for the adsorption of PTM-NPs to determine both change in enthalpy and entropy (19) The Arrhenius equations were used to evaluate the kinetics and thermodynamics parameters for the corrosion of Mild steel in 1.0 M HCl in the absence and presence of PTM-NPs using Equations 6 and 7 (3); (11); (23); (30)

$$Log CR = log A - \left(\frac{E_a}{2.303RT}\right)$$

$$Log\left(\frac{CR}{T}\right) = \left[\left(log\left(\frac{R}{Nh}\right) + \left(\frac{\Delta S^*}{2.303R}\right)\right)\right] - \frac{\Delta H^*}{2.303RT}$$
(6)

Where  $E_a$  denotes activation energy, A is the Arrhenius frequency factor, R is the universal gas constant, and T is absolute temperature,  $\Delta H^*$  is activation enthalpy, and  $\Delta S^*$  is activation entropy. The activation energy  $E_a$  is obtained from the slope of log CR vs. 1/T, while  $\Delta H^*$  and  $\Delta S^*$  are determined from the slope and intercepts of plots of  $Log\left(\frac{CR}{T}\right) vs \frac{1}{T}$  respectively (3)

The  $\boldsymbol{E}_{\boldsymbol{a}}$  and  $\Delta H^*$  values in the presence of PTE-Ag and AIE-Ag are higher than that of the PTE-TiNPs and AIE-TiNPs. Activation energy increases with the presence of transitional metals (Ag and Ti) loading and Ag inhibits better than the Ti nanoparticles. Similar results have been reported in literature (3). These findings align with recent studies which reported similar observations, where Ag-based nanoparticles exhibited superior corrosion resistance compared to their Ti-based counterparts due to higher energy barriers for metal dissolution (4); (8). According to collision theory, the increased activation energy in the presence of inhibitors suggests that the energy barrier for acid attack on the mild steel surface is elevated, thus slowing down the corrosion process. Furthermore, the negative values of  $\Delta S^*$  observed for PTM-NPs imply that the formation of the activated complex involves an association step, leading to a more ordered transition state. This supports the adsorption mechanism, where the system becomes more ordered during the formation of the inhibitor-metal interface (23); (10).

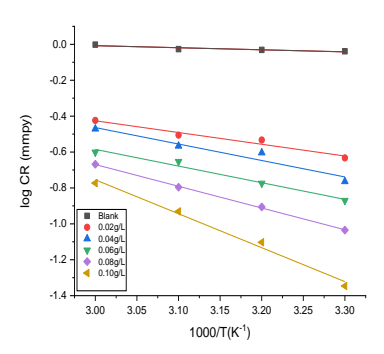


**Figure 23.** Arrhenius plot for inhibition of mild steel corrosion in 1.0 M HCl without and with different concentrations of PTE-AgNPs

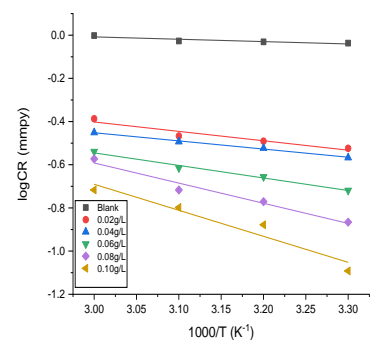


**Figure 24.** Arrhenius plot for inhibition of mild steel corrosion in 1.0 M HCl without and with different concentrations of PTE-TiNPs

#### **CONCLUSION**

From the study, it can be concluded that the plant extracts, PTM-NPs all inhibited the corrosion of mild steel in 1.0 M HCl.

It was observed that the inhibition efficiencies increased with increasing concentrations of the inhibitors and reaches maximum at 0.10 g/L.

The transition metal nanoparticles inhibits more than the crude extracts, with PTE-AgNPs having the highest inhibition efficiency of (95.1%) followed by PTE-TiNPs (91.2%) and PTE being (87.7%).

However, the corrosion inhibition decreased with increase in temperature for all inhibitors. This is because the molecular activation becomes greater, which leads to an increase in corrosion rate.

The adsorption of PTE and PTM-NPs on mild steel was spontaneous, involving physical interactive forces and best described by the Langmuir adsorption isotherm.

PTM-NPs act as mixed type of inhibitor with anodic predominance from the potentiodynamic polarization result. Hence, PTM-NPs serve as a better inhibitor as compared with the crude plant extracts (PTE)

#### Acknowledgement

We thank God almighty for the success of this studies, and all the technologists and researchers that contributed to this reach work.

#### REFERENCES

Adewuyi, A., Adedeji, O., & Awolola, G. (2022). Green synthesis of metal oxide nanoparticles using plant extracts: Characterization and application in corrosion inhibition. *Materials Today: Proceedings*, *56*, 2055–2061. <a href="https://doi.org/10.1016/j.matpr.2022.03.479">https://doi.org/10.1016/j.matpr.2022.03.479</a>

Afolayan, M., Srivedavyasasri, R., Asekun, O. T., Familoni, O. B., Orishadipe, A., Zulfiqar, F., & Ross, S. A. (2018). Phytochemical study of *Piliostigma thonningii*, a medicinal plant grown in Nigeria. *Medicinal Chemistry Research*, 27, 2325–2330.

Ali, H. E., Al-Faheem, H. H., & El-Lateef, H. M. A. (2021). Thermodynamic and kinetic evaluation of ecofriendly inhibitors for mild steel corrosion in acidic medium. *Journal of Molecular Liquids*, *334*, 116066. https://doi.org/10.1016/j.molliq.2021.116066

Al-Otaibi, M. S., Al-Senani, G., & Al-Kahtani, A. A. (2022). Comparative analysis of silver and titanium nanoparticles as corrosion inhibitors in acidic medium: Thermodynamic and kinetic approach. *Journal of Materials Research and Technology*, 20, 1390–1400. https://doi.org/10.1016/j.jmrt.2022.08.104

Arun Sundaram, B., Kesavan, K., & Parivallal, S. (2018). Recent advances in health monitoring and assessment of

in-service oil and gas buried pipelines. *Journal of The Institution of Engineers (India): Series A*, 99, 729–740.

Bibi, I., Nazar, N., Iqbal, M., Niazi, N. K., Athar, M., Bashir, S., ... & Shaheen, S. M. (2021). Green synthesis of iron oxide nanoparticles using *Ziziphus mauritiana* leaf extract: Characterization and evaluation for antimicrobial, antioxidant and catalytic potential. *Environmental Research*, *195*, 110652. https://doi.org/10.1016/j.envres.2021.110652

Daoudi, W., El Aatiaoui, A., Falil, N., & Adyl, O. (2023). Sustainable approach for corrosion control in mild steel using plant-based inhibitors: A review. *Materials Today Sustainability*, 22, 100373. https://doi.org/10.1016/j.mtsust.2023.100373

El-Naggar, M. M., Fouda, A. S., & El-Haddad, M. N. (2022). Temperature influence on the adsorption and inhibition behavior of green-synthesized nanoparticles on steel surfaces. *Surface Interfaces*, *28*, 101662. https://doi.org/10.1016/j.surfin.2022.101662

Eltaweil, A. S., Elgarhy, G. S., El-Subruiti, G. M., & Omer, A. M. (2021). Effective adsorption of Pb(II) from aqueous solution by a novel green synthesized magnetic nanoparticles: Adsorption process optimization with artificial intelligence and mechanism investigation. *Journal of Hazardous Materials*, 403, 123693. https://doi.org/10.1016/j.jhazmat.2020.123693

El-Etre, A. Y., Abdallah, M., & Mousa, M. A. (2022). Thermodynamic and kinetic assessment of novel plant extract-derived inhibitors for mild steel in acidic media. *Corrosion Science*, 199, 110177. <a href="https://doi.org/10.1016/j.corsci.2022.110177">https://doi.org/10.1016/j.corsci.2022.110177</a>

El-Naggar, N. E., Hussein, M. H., El-Sawah, A. A., & Fouda, M. M. (2021). Impact of biosynthesized copper oxide nanoparticles on *Bacillus subtilis* for plant growth promotion and suppression of soilborne pathogens. *Scientific Reports*, 11, 14778. https://doi.org/10.1038/s41598-021-94213-3

Essien, E. A., Kavaz, D., Ituen, E. B., & Umoren, S. A. (2018). Synthesis, characterization and anticorrosion property of olive leaves extract—titanium nanoparticles composite. *Journal of Adhesion Science and Technology*, *32*(16), 1773–1794.

Ezzat, O. A., Aigbodion, V. S., Al-Lohedan, H. A., & Ozoude, C. J. (2024). Silver nanoparticles from *Anacardium occidentale* leaf extract for corrosion inhibition of mild steel in seawater. *RSC Advances*, 14(26), 18395–18405.

https://doi.org/10.1039/D4RA01234A

Faes, W., Lecompte, S., Ahmed, Z. Y., Van Bael, J., Salenbien, R., Verbeken, K., & De Paepe, M. (2019). Corrosion and corrosion prevention in heat exchangers. *Corrosion Reviews*, *37*(2), 131–155.

Fernandes, C. M., Alvarez, L. X., dos Santos, N. E., Barrios, A. C. M., & Ponzio, E. A. (2019). Green synthesis of 1-benzyl-4-phenyl-1H-1,2,3-triazole, its application as corrosion inhibitor for mild steel in acidic medium and new approach of classical electrochemical analyses. *Corrosion Science*, 149, 185–194.

Gholami, R. S., Naderi, R., Mahdavian, M., & Rostami, M. (2020). *Dysphania ambrosioides* essential oil as a green corrosion inhibitor for mild steel in hydrochloric acid solution. *International Journal of Chemical and Biochemical Research*, 6(1), 1–12.

Ghosh, S., Bose, S., & Das, M. (2023). Temperature effect on the adsorption and inhibition properties of green corrosion inhibitors on mild steel in acidic medium. *Journal of Molecular Liquids*, *381*, 121771. https://doi.org/10.1016/j.molliq.2023.121771

Islas, J. F., Acosta, E., Zuca, G., Delgado-Gallegos, J. L., Moreno-Treviño, M. G., Escalante, B., & Moreno-Cuevas, J. E. (2020). An overview of Neem (*Azadirachta indica*) and its potential impact on health. *Journal of Functional Foods*, 74, 104171.

Ituen, E. B., Udoinyang, E. E., Udoetok, I. A., & Ita, B. I. (2022). ZrO<sub>2</sub>—glycine nanocomposite as an eco-friendly corrosion inhibitor for mild steel in acidic medium. *Progress in Chemical and Biochemical Research*, *5*(2), 122–132. <a href="https://doi.org/10.48309/pcbr.2022.172942">https://doi.org/10.48309/pcbr.2022.172942</a>

Khan, M. A., Shaik, M. R., Adil, S. F., Kuniyil, M., Assal, M. E., Tahir, M. N., ... & Khan, M. (2022). Plant-extract-assisted green synthesis of transition metal nanoparticles for sustainable applications: A review. *ACS Sustainable Chemistry & Engineering*, 10(8), 2664–2682. https://doi.org/10.1021/acssuschemeng.1c07280

Kokalj, A. (2022). Corrosion inhibitors: Physisorbed or chemisorbed? *Corrosion Science*, 196, 109939.

Murugesan, S., Dhulipala, P., Liu, Z., & Ramachandran, S. (2020, June). Nanotechnology-based field method for detection and monitoring of corrosion inhibitors. In *CORROSION* 2020. OnePetro.

Obot, I. B., Macdonald, D. D., & Umoren, S. A. (2023). Recent insights into the kinetics and thermodynamics of corrosion inhibition using green materials. *Electrochimica Acta*, 453, 141262.

https://doi.org/10.1016/j.electacta.2023.141262

Olasehinde, O., Adeyemo, A. O., Olasunkanmi, L. O., & Obot, I. B. (2022). Synthesis and evaluation of *Chromolaena odorata*—TiO<sub>2</sub> nanocomposites as corrosion inhibitors for mild steel in 1.0 M HCl. *Materials Chemistry and Physics*, 275, 125223. https://doi.org/10.1016/j.matchemphys.2021.125223

Omole, M. A., Olasunkanmi, L. O., & Ebenso, E. E. (2022). Corrosion inhibition performance of green synthesized metal nanoparticles: Recent advances and future perspectives. *Journal of Molecular Liquids*, *360*, 119502. https://doi.org/10.1016/j.molliq.2022.119502

Oyebamiji, O. B., Fakunle, P. B., & Ogunlaja, A. S. (2022). Bio-mediated synthesis of silver and titanium oxide nanoparticles using plant extracts for corrosion inhibition of mild steel in acidic medium. *Journal of Molecular Structure*, 1261, 132914. <a href="https://doi.org/10.1016/j.molstruc.2022.132914">https://doi.org/10.1016/j.molstruc.2022.132914</a>

Osama Ezzat, A., Aigbodion, V. S., Al-Lohedan, H. A., & Ozoude, C. J. (2024). Silver nanoparticles from *Anacardium occidentale* leaf extract for corrosion inhibition of mild steel in seawater. *RSC Advances*, 14(26), 18395–18405. https://doi.org/10.1039/D4RA01234A

Rajendran, S., Gunasekaran, G., & Abbas, M. A. (2021). Bioengineered silver nanoparticles as green corrosion and biofilm inhibitors in cooling water systems. *Environmental Science and Pollution Research*, 28, 4761–4772.

https://doi.org/10.1007/s11356-020-11085-w

Rajiv, P., Saranya, M., Venckatesh, R., & Rajeshwari, S. (2021). Green synthesis and characterization of zinc oxide nanoparticles using plant extract and evaluation of their anti-corrosive and antibacterial properties. *Journal of Materials Science: Materials in Electronics*, 32(12), 16120–16130. <a href="https://doi.org/10.1007/s10854-021-06290-0">https://doi.org/10.1007/s10854-021-06290-0</a>

Saleh, M. M., El-Deeb, M. M., & Fekry, A. M. (2024). Temperature dependence of corrosion inhibition of steel in acidic media by plant-derived nanocomposites. *Corrosion Science*, 220, 111022. <a href="https://doi.org/10.1016/j.corsci.2023.111022">https://doi.org/10.1016/j.corsci.2023.111022</a>

Sathiyanathan, S., Jeyasundari, J., & Raj, P. A. (2023). Green synthesis of chitosan–AgNPs composite using *Rumex vesicarius* extract for mild steel corrosion inhibition in CO<sub>2</sub> environment. *Journal of Molecular Liquids*, 373, 121030. https://doi.org/10.1016/j.molliq.2023.121030

Verma, C., Quraishi, M. A., & Rhee, K. Y. (2022). Natural ligands: Promising ecofriendly alternatives for corrosion protection and plethora of many prospects. *Process Safety and Environmental Protection*, *162*, 253–290.

Zuo, Y., Wang, J., & Li, L. (2023). Corrosion inhibition of mild steel by black mustard seed and *Ganoderma lucidum* extracts in acidic and saline media. *Surface Engineering and Applied Electrochemistry*, 59, 210–217.